ELSEVIER

Earth and Planetary Science Letters 144 (1996) 435–451

EPSL

Metamorphism and deformation along the emplacement thrust of the Samail ophiolite, Oman

B.R. Hacker *, J.L. Mosenfelder

Department of Geological and Environmental Sciences, Stanford University, Stanford, CA 94305-2115 USA

Received 3 January 1996; revised 11 September 1996; accepted 14 September 1996

Abstract

The base of the Samail ophiolite is a metamorphic shear zone that provides key information about ophiolite emplacement. The classic exposure of this metamorphic sole at Wadi Tayin consists of a few meters of garnet–clinopyroxene mafic gneiss and 80 m of upper amphibolite facies mafic and quartzose tectonite, overlying 150 m of lower amphibolite facies mafic and sedimentary schist. The sole is bounded by faults but is internally coherent. Peak metamorphic temperatures decrease exponentially, from ~ 825°C at the top of the sole to ~ 500°C at its base, as documented by changes in grain size, hornblende composition, the disappearance of chlorite and epidote, garnet–clinopyroxene element partitioning, and garnet–hornblende partitioning. The inverted peak temperature gradient decreases from > 4000°C/km in the upper 50 m to ~ 100°C/km in the lower 150 m. Contrary to earlier reports, greenschist-facies tectonites are not present at Wadi Tayin, although the entire sole underwent greenschist-facies retrogression, driven by the influx of fluids from the overlying peridotite or underlying carbonate. Calculations based on an amphibolite constitutive relation reveal that, although the section represents a lithologic continuum, the lower 200 m of the sole is a relatively undeformed block whereas the uppermost 25 m represent material initially separated by tens to a couple of hundreds of kilometers and now integrated into a single column.

Keywords: ophiolite; emplacement; prograde metamorphism; retrograde metamorphism; subduction; United Arab Emirates; Oman

1. Introduction

One of the mysteries of plate tectonics is how ophiolites with densities of 3.0–3.3 g/cm^3 are raised from their natural depths of ≥ 2.5 km beneath the ocean surface to elevations more than 1 km above sea level on continents with densities of 2.7–2.8 g/cm^3. This question is most profound for ophiolites emplaced onto continental margins, such as the Samail ophiolite.

There are two basic models for the emplacement of the Samail ophiolite: an 'arc' model and a 'ridge' model. In the ridge model [1] the ophiolite represents one limb of an oceanic spreading center that was forced over the opposite limb and onto the Arabian continent. The arc model [2] suggests that the ophiolite originated as an intraoceanic arc that rode over subducting oceanic lithosphere and onto the Arabian continent.

One of the most striking aspects of the Samail ophiolite is a thin sliver of metamorphic rocks that

* Corresponding author. Present address: Geology Department, University of California at Santa Barbara, Santa Barbara, CA 93106-9630, USA. E-mail: hacker@magic.geol.ucsb.edu

PII S0012-821X(96)00186-0

comprises a high-temperature shear zone beneath the ophiolite. This sole thrust has been reported to contain amphibolite and greenschist facies rocks that record an inverted thermal gradient of $> 1000°C/km$ [3]. In this paper we demonstrate that the gradient is exponential and developed syntectonically under exclusively amphibolite-facies conditions.

2. Overview of the Samail ophiolite

The Samail ophiolite of the Sultanate of Oman and the United Arab Emirates is the best exposed and least deformed ophiolite in the world (Fig. 1). It is one of the largest thrust sheets on Earth, with a length of > 400 km, a width of 150 km, and an inferred pre-emplacement thickness of 15–20 km (Fig. 2). The genesis of the Samail ophiolite is somewhat uncertain. Although there is agreement that the uppermost, volumetrically least significant lavas erupted from intraplate seamounts, the lower and middle volcanics have been interpreted as supra-subduction zone lavas [2,4], or, alternatively,

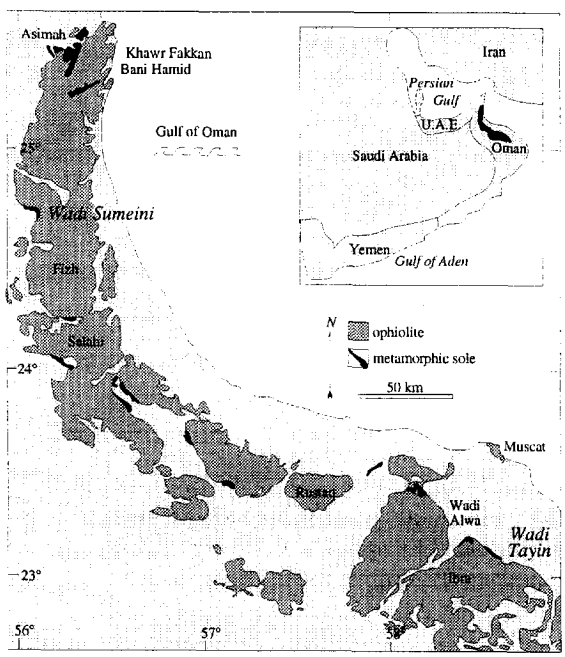

Fig. 1. Map of the Samail ophiolite, showing the locations of Wadi Sumeini and Wadi Tayin. The metamorphic sole crops out over the length and breadth of the ophiolite.

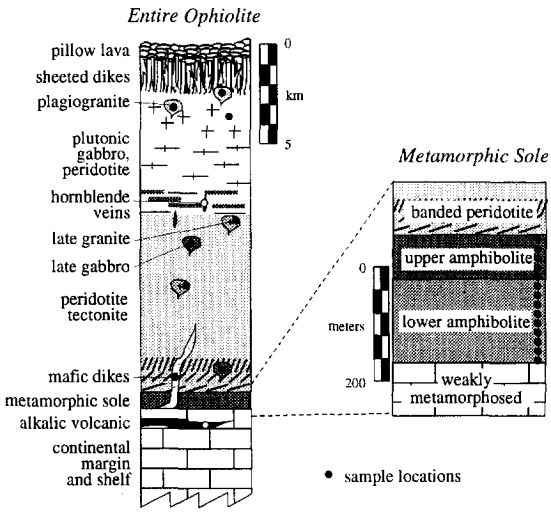

Fig. 2. Interpretive pseudostratigraphic section through the Samail ophiolite (based on [2,15,35–37]); locations of rocks samples for petrological and geochronological study are shown.

as the products of mid-ocean-ridge spreading and subsequent intraoceanic thrusting [5,6].

The Samail ophiolite was thrust over adjacent oceanic lithosphere and then onto the Arabian craton along a several hundred meter thick shear zone, or 'metamorphic sole'. This sole has been described as partially melted amphibolite grading downward into greenschist facies sedimentary and mafic rocks [3,7,8]. Immediately underlying the sole are relatively unmetamorphosed metasedimentary and metavolcanic rocks from a Triassic to Late Cretaceous passive margin and ocean basin that lay northeast of the Arabian craton [2,9,10]. The amphibolite is believed to represent mafic oceanic crust overridden during the early, intraoceanic thrusting stage of emplacement, whereas the greenschists are inferred to be basalt, clastic sediment, and chert overridden at a later stage [7].

The least disrupted exposures of the sole contain ~ 200 m of rocks formed at peak temperatures ranging from 500° to 800°C [3,11]. This indicates a metamorphic field gradient of $> 1000°C/km$ — a factor of 10 steeper than thermal gradients produced in conventional thermal models of subduction zones. Such unusually steep inverted metamorphic gradients require a special means of formation, such as syn-metamorphic downward propagation of a shear zone

[12,13]. The objective of this study was to evaluate whether the metamorphism and deformation of the sole exhibit smooth or discontinuous gradients, as these characteristics reveal the tectonic process involved in forming the sole.

3. Metamorphism and deformation of the sole

We visited two well described sections of the sole: Wadi Tayin and Wadi Sumeini (Fig. 1). We focused our work on the classic Tayin section, where we completed a large-scale map with the aid of a measuring tape, compass, GPS receiver, and aerial photographs (Fig. 3A). This inspection revealed that the sole is cut by rare high-angle faults with offsets on a scale of a few meters to tens of meters, but otherwise is structurally coherent. We then collected samples along transects through the sole.

Alleman and Peters [14] described the sole as an upper 'polymetamorphic' amphibolite facies series overprinted by greenschist facies metamorphism, and a lower 'monometamorphic' greenschist facies series. The outcrop at Tayin consists of three readily differentiable zones (Fig. 3). The uppermost few meters are coarse-grained hornblende + clinopyroxene + garnet gneiss with very rare pods of partial melt composed of plagioclase + quartz + apatite ± epidote ± hornblende ± clinopyroxene. Below that are 80 m of medium-grained, gneissic to schistose hornblende + plagioclase rocks with rare carbonate and muscovite-bearing calc-silicate layers up to 1 m thick and more abundant quartzose layers up to 13 m thick. These various rock types are locally intermixed at the centimeter scale. Axial planes and fold hinges of isoclinal folds (on a scale of centimeters to decimeters) parallel the foliation and stretching lineation, respectively. The protolith for most of the quartzose rocks was probably chert, based on their association with mafic oceanic rocks; abundant constituent quartz with less muscovite, iron oxides, and minor plagioclase; and the presence of chert beneath the sole.

The upper amphibolite facies zone grades down into the lowermost zone, which is 150 m thick and formerly referred to as "greenschist and light green phyllite to slate" (e.g., 3). It is green to greenish–black schist and phyllite composed of fine-grained hornblende + plagioclase + chlorite, with widespread < 1 m thick quartzose and muscovite-bearing calc-silicate layers. The quartzose layers have abundant millimeter-scale transposed quartz veins, and similar veins are evident within nearby mafic rocks. A variety of folds are present. Kink- or box-fold crenulations, a few millimeter to centimeters long are found in domains smaller than 1 m in length. Other domains that cut the foliation at high angles contain centimeter to decimeter scale isoclinal to tight refolds of the high-temperature foliation. They are usually associated with high-angle faults and are locally dissected by quartz veins. Ghent and Stout [3] reported that the lowermost zone of the sole contains the greenschist facies assemblage chlorite + actinolite + epidote + quartz + albite + calcite, but we present data below that contradict this and, instead, indicate lower amphibolite facies conditions.

The upper contact of the sole with the overlying serpentinized banded ultramafic unit is a gently folded high-angle fault that truncates amphibolite-facies foliation within the sole [3]. Rodingite with hydrogrossular, prehnite, clinozoisite and carbonate occurs within 1–2 m of the peridotite [3]. A sharp contrast in metamorphic grade indicates that the lower contact of the sole with the underlying Umar Group is also a fault. Chert in the Umar Group contains radiolaria ghosts and unrecrystallized mafic volcaniclastic rocks deformed by low temperature fracture and slip along small-scale brittle faults. In contrast to this, no igneous or sedimentary features are preserved in the sole. Boudier et al. [1,8,15] measured lineations and quartz lattice preferred orientations at Tayin and concluded that the thrusting direction was westward in the amphibolite and southwestward in the fine-grained amphibolite; however, we found no consistent change in foliation or lineation orientation between the coarse and fine-grained amphibolite (Fig. 3B).

The dominant amphibolite facies mineral parageneses are overprinted by greenschist and prehnite–pumpellyite facies minerals [3]. Minor actinolite to actinolitic hornblende is abundant in the upper half of the section. Albite partially to completely replaces plagioclase in all mafic rocks; the most pervasive alteration of plagioclase occurs in the first 20 m beneath the peridotite. Rocks low in the section previously mapped as greenschist actually contain

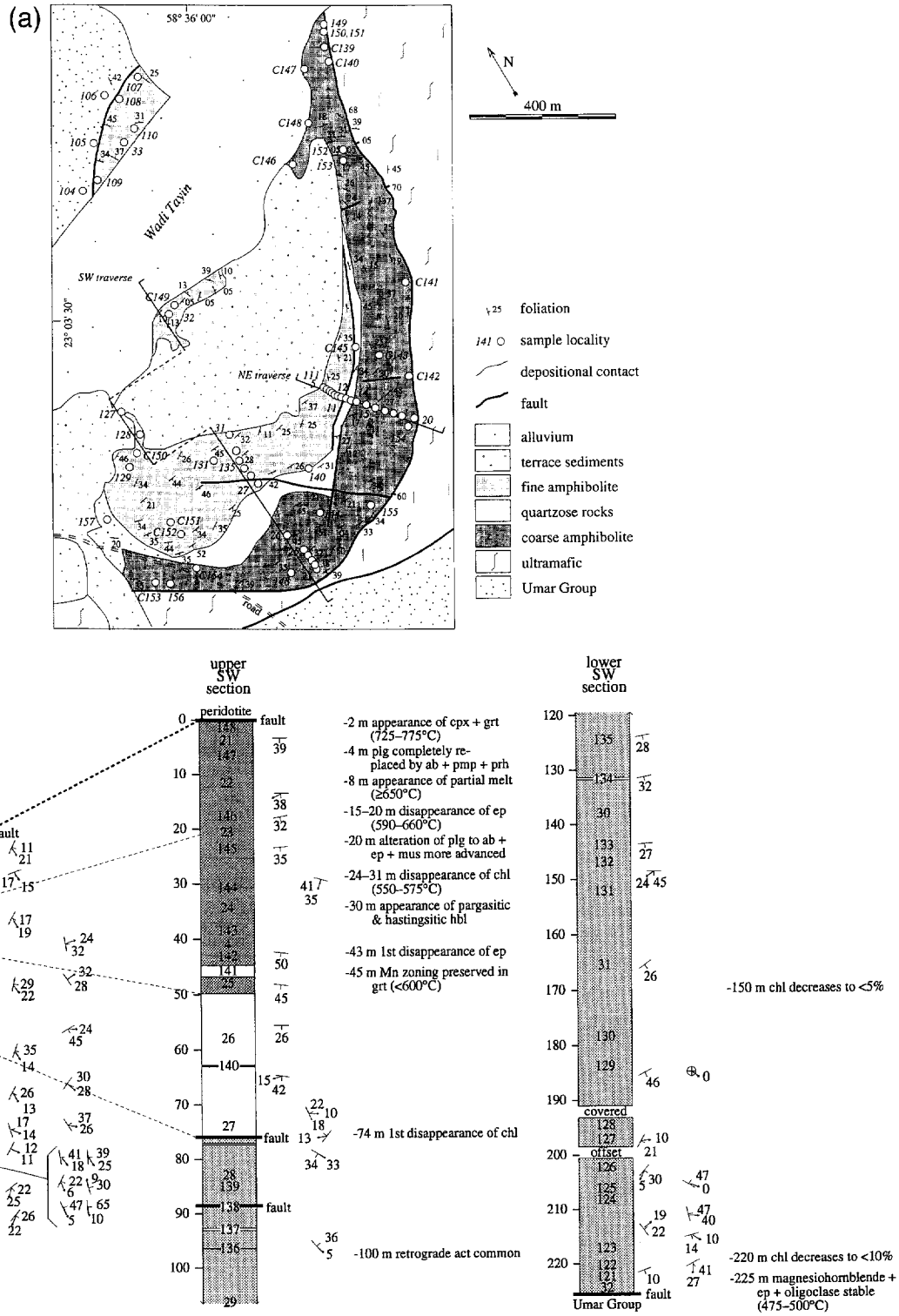
(a)
58° 36' 00"
23° 03' 30"
Wadi Tayin
SW traverse
NE traverse
road
N
400 m
foliation
sample locality
depositional contact
fault
alluvium
terrace sediments
fine amphibolite
quartzose rocks
coarse amphibolite
ultramafic
Umar Group
(b)
NE section
peridotite
fault
terrace gravel
upper SW section
peridotite
fault
fault
fault
-2 m appearance of cpx + grt (725–775°C)
-4 m plg completely replaced by ab + pmp + prh
-8 m appearance of partial melt (≥650°C)
-15–20 m disappearance of ep (590–660°C)
-20 m alteration of plg to ab + ep + mus more advanced
-24–31 m disappearance of chl (550–575°C)
-30 m appearance of pargasitic & hastingsitic hbl
-43 m 1st disappearance of ep
-45 m Mn zoning preserved in grt (<600°C)
-74 m 1st disappearance of chl
-100 m retrograde act common
lower SW section
covered
offset
fault
Umar Group
-150 m chl decreases to <5%
-220 m chl decreases to <10%
-225 m magnesiohornblende + ep + oligoclase stable (475–500°C)

the smallest proportion of greenschist facies minerals.

4. Deformation textures at Wadi Tayin

In spite of the appearance that the sole grades from amphibolite at the top to greenschist at the bottom, virtually all mafic rocks contain the same paragenesis of hornblende + plagioclase. The apparent change in metamorphic facies is the result of increasing chlorite content, smaller grain size, and a more nematoblastic habit of amphibole lower in the section. Amphibole crystals coarser than 200 μm all lie within 130 m of the peridotite, and no grains smaller than 50 μm are found within 40 m of the peridotite. Low in the section amphiboles are green and nematoblastic, whereas at the top of the section they are brown and prismatic to equant. Common to all samples is a high-temperature texture consisting of hornblende with weak undulatory extinction and limited or no subgrain development at crystal margins, and plagioclase with weak undulatory extinction and weak to moderate mechanical twinning. Recrystallization of hornblende in these samples was coincident with isoclinal folding. This high-temperature texture is locally overprinted by a porphyroclastic texture in which the hornblende crystals show moderate to strong undulatory extinction, microcracking, domino-style rotation, and growth of actinolite in strain shadows. Plagioclase grains are deformed into δ clasts by a combination of microcracking and recrystallization, and epidote grains comprise recrystallized σ clasts.

Greenschist facies deformation of the mafic rocks is insignificant except at the upper and lower boundaries of the sole. Greenschist facies alteration of amphibolite facies minerals is locally pervasive [3], but the alteration minerals are relatively undeformed throughout the bulk of the section. Greenschist facies veins developed by cracking of amphibolite facies minerals show shear displacements of ≤ 1 dm. Low-temperature cracking and brittle sliding accompanied by zeolite growth is weakly developed along the contact with the peridotite.

Quartz grains present two separable fabric types: earlier high-temperature features are overprinted by a low-temperature fabric. The amphibolite facies fabric consists of subequant, tabular quartz grains with either well recovered, gently curved boundaries, or dentate boundaries formed by limited grain-boundary migration (Fig. 4A). The absence of flattened grains and the presence of smoothly varying undulatory extinction indicate that dislocation recovery was accommodated by dislocation climb. Quartzose rocks preserve evidence of concomitant dissolution and redeposition (Fig. 4B). Quartz ± calcite ± epidote veins range from relatively undeformed and subperpendicular to foliation, to transposed, nearly parallel to the foliation. Quartz grains in the veins have textures similar to the host rock, and indicate deformation by dislocation creep. Phyllosilicate-rich layers within quartzose rocks have stylolitic teeth, contain other insoluble phases, and offset and truncate quartz veins. Calcite veins increase in abundance down section, suggesting that the underlying carbonate-rich Umar Group was their source. The dislocation creep and solution transfer features developed coevally and are present from top to bottom of the section. In domains where the high-temperature foliation was refolded, a weak greenschist facies deformation consists of moderate undulatory extinction, weak deformation bands, and weak development of ribbon grains.

Many of the metasedimentary rocks contain evenly dispersed muscovite grains < 50 μm in diameter. With rare exceptions, these phyllosilicates pin quartz grain boundaries, preventing the development of an equilibrium grain size that might potentially yield information regarding paleostress or temperatures of

Fig. 3. (A) Map of the Green Pool area along Wadi Tayin, based on this study and unpublished mapping by R.G. Coleman and R.T. Gregory (reproduced by Ghent and Stout [3]); locations of NE and SW geologic traverses are shown. (B) Sections through NE and SW traverses of the metamorphic sole at Wadi Tayin. Rock types as (A). Sample numbers are shown in the center of each column, and structural thickness to the left (meters). The first column of structural measurements are strike and dip of foliation and trend and plunge of lineation, while the second column of structural measurements are strike and dip of fold hinge surfaces and trend and plunge of fold axes; the column most to the right describes changes in mineralogy and texture of the mafic rocks.

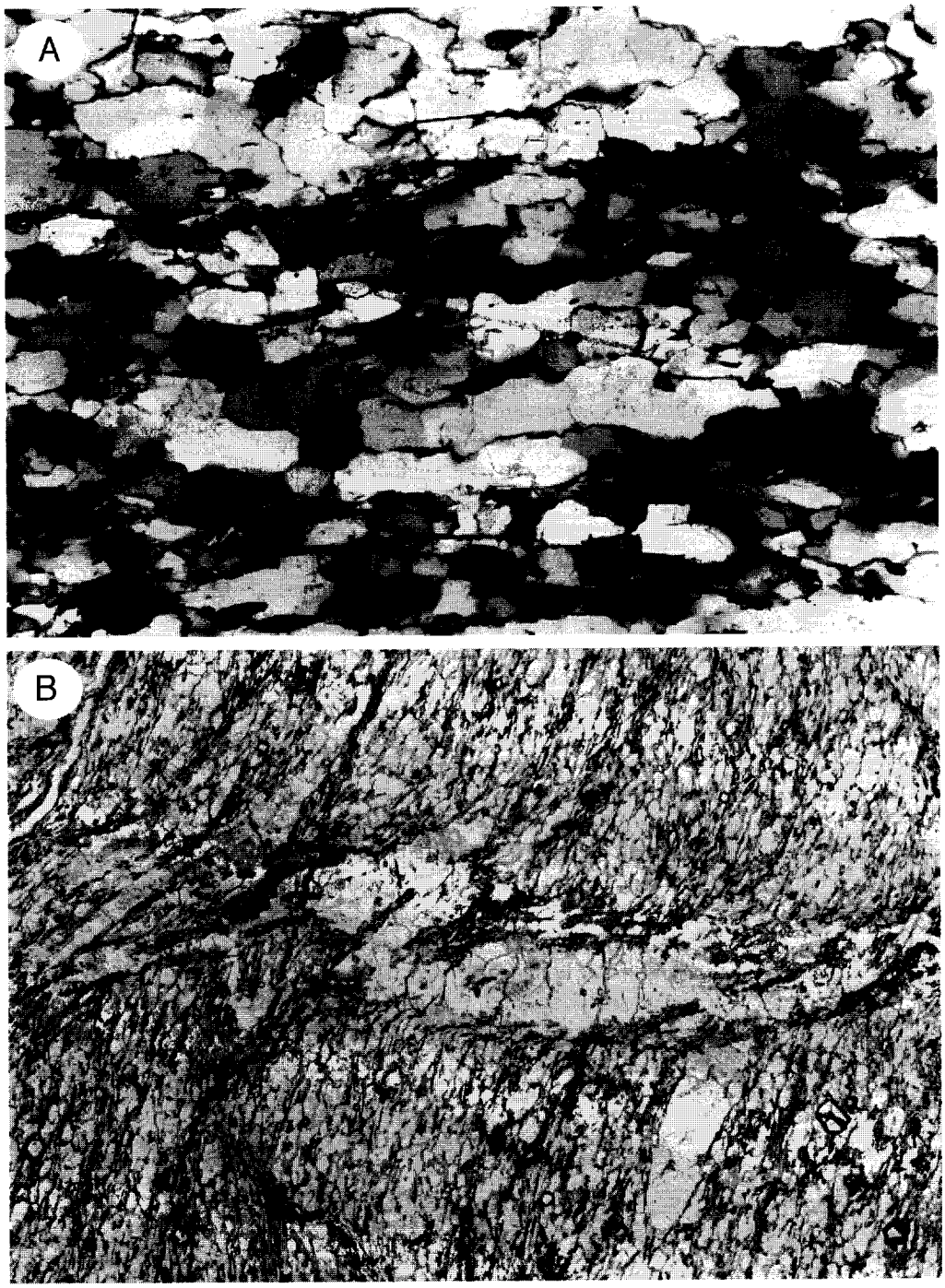

Fig. 4. Photomicrographs of quartz textures; field of view is 3.5 mm. (A) Subequant, tabular quartz grains with well-recovered, gently curved boundaries; crossed polars. (B) Quartz vein nearly orthogonal to foliation; uncrossed polars.

grain growth. For the same reason, quartz grain size does not vary systematically with structural position in the sole.

5. Mineral textures and compositions

Sixteen of ~350 samples collected from Tayin and Sumeini were analyzed by electron microprobe (Tables 1–3).

5.1. Feldspar

Every mafic rock from the sole contains micron-sized albite (An_{05}–An_{09}) formed during retrogression, and less frequently, calcic plagioclase relicts from peak metamorphism (Table 1). Relict plagioclases are as calcic as An_{54}. We can identify no relationship between plagioclase composition and the presence or absence of other minerals. Retrogressed calcic plagioclases are replaced by intergrowths of albite, K-feldspar, epidote or pumpellyite, and muscovite throughout the entire section, except for 3–4 m below the peridotite, where plagioclase is completely replaced by albite + pumpellyite + prehnite. Alkali feldspar is not a peak metamorphic phase, and is present only as an alteration product of plagioclase or in veins.

5.2. Amphibole

Amphiboles formed during two stages of metamorphism (Table 2). Hornblende grown during amphibolite facies metamorphism is present throughout the sole. The bulk of the section (lower 200 m of 230 m) consists of green magnesiohornblende and tschermakitic hornblende that vary little in composition; the upper 30 m contain brown ferroan pargasitic hornblende and magnesian hastingsitic hornblende. No systematic compositional zoning was observed in the hornblendes sensu stricto, although actinolite to actinolitic hornblende overgrowths formed during greenschist facies metamorphism are prevalent at the top of the section and uncommon in the lower 100 m. In contrast to previous reports, the Tayin section of the sole does not contain actinolite formed during prograde or peak metamorphic conditions.

There are systematic changes in amphibole composition with structural position in the sole (Fig. 5). An upward increase in TiO_2 has been noted at Sumeini [11] and Tayin [3]. At Tayin, hornblende TiO_2 content is relatively constant in the lower 200 m, but increases markedly to >2.5 wt% in the uppermost 10 m (Fig. 5A). This could be the result of a rapid increase in peak metamorphic temperature [16] or it could be because the stable Ti-rich phase changes from ilmenite to rutile. K_2O is the only oxide in hornblende that increases upward through the entire section (Fig. 5B); hornblendes from sample C142 are particularly rich in K_2O, reaching 1.5 wt%. An upward increase in amphibole FeO/MgO noted at Sumeini [11], is not present at Tayin (Fig. 5C), where actinolites exhibit an upward *decrease* in FeO/MgO. The Al_2O_3 content of hornblende shows a weak up-section increase, whereas actinolites show the reverse relationship (Fig. 5D).

5.3. Clinopyroxene

Clinopyroxene occurs commonly in mafic rocks within 2 m of the peridotite. It occurs as much as 80 m beneath the mantle section [3], but only locally, indicating a bulk compositional control. Orthopyroxene was not found. Clinopyroxene compositions are nearly invariant, with 44–50 mol% $CaSiO_3$, 34–37 mol% $MgSiO_3$, and 12–21 mol% $FeSiO_3$ (Table 3). Other minor components are Al_2O_3: 2.5–5.0 wt%, TiO_2: 0.2–0.6 wt%, MnO: 0.1–0.5 wt%, and Na_2O: 0.5–0.9 wt%. Systematic zoning was not observed in clinopyroxene, except for depressed Fe/Mg ratios along the rims of some crystals adjacent to or included within garnet.

5.4. Garnet

In the mafic rocks garnet is uncommon and occurs only in the structurally highest portions of the sole, within 2 m of the overlying peridotite [3], where it coexists with hornblende + plagioclase + clinopyroxene. Three different compositions of garnet are observed in the mafic rocks (Table 3): hydrogrossular, $Alm_{25}Pyr_{00}Gro_{74}Sps_{01}$, in rodingite [11]; Ca–Mn rich garnets, $Alm_{30}Pyr_{08}Grs_{40}Sps_{22}$, in discrete veins lacking other ferromagnesian phases; and almandine-rich garnets, $Alm_{45-56}Pyr_{15-24}Grs_{17-34}Sps_{01-08}$, as a peak metamorphic phase. Most have unzoned or weakly zoned interiors that we interpret as reflecting homogeniza-

Table 1
Mineral assemblages in Oman mafic rocks examined in detail by back-scattered electron imaging and electron-probe microanalysis

Sample	Plg	Hbl Core	Hbl Rim	Wo,En,Fs	Al,Py,Sp,Gr	Ms	Ep	Bt	Chl	Pmp	Prh	Py	Mag	Rt	Spn	Ilm	Hem	Cal	Qtz	Zeol
C139	Ab	**FnPgHb**	Act	**44,39,18**	**56,24,02,17**	3.2	22,23		·	·	·	·			·	●		·		·
C142	Ab	**Ts**	Act	**50,39,12**	**30,08,22,40**	3.2	07,21		67	·					·,●			·		
C153	Ab	**FnPgHb**	**FnPgHb**	**47,36,17**	**49,22,03,23**	3.2	17			·				●	·	●	·	·		
O5	Ab, **34**	**MgHb**	Act			3.3	●	·	74, ●				●	●		●	·	·		
O11	Ab,**24**	**MgHb**	**MgHb**			3.2	**2.2,** ·		76					●	·					
O16	Ab	**TsHb**	Act			3.1	**21,** ●		72,●						·, ●		·			
O19	Ab,**47**	**MgHb**	**MgHb**	**49,38,13**		3.2	02,06		·	·			●		·, ●		·			
O21	Ab,**30**	**PgHb**	Act	**48,36,16**		3.3			·	·					·,●		·	·		
O25	Ab,**54**	**MgHb**	Act			3.3	**22**		·	·				●	·		·			
O30	Ab,**23**	**TsHb**	Act			3.2	**20,** ·		·, ●					●				·	·	
O31	Ab	**TsHb**	**MgHb**				**24–29,** ·		·, ●								·	·		
O32	Ab	**MgHb**	**MgHb**			3.3	**28,** ·		·,●								·	·	·	
O33	Ab,**12**	**MgHb**	**MgHb**				**25,** ·		·				●		·	●		·	·	
O54		**TsHb**	Act	**48,34,18**	**45,20,03,28**		29				·	·			·					
O56		**TsHb**	**TsHb**	**46,37,17**	**52,20,08,17**		·		·		·				·		·			
O156	Ab	**PgHb**	Act	**48,35,17**	**48,15,05,32**	·	·			·				·	·		·			

Prograde minerals are in bold or marked by ●, retrograde are in normal type or marked by ·. Plg shows presence or absence of albite and An content of other plagioclase. Hbl core and hbl rim indicate compositions of hornblende core and rim; Ts = tschermakite; FnPgHb = ferroan pargasitic hornblende; MgHb = magnesio-hornblende; TsHb = tschermakitic hornblende; Act = actinolite; Wo,En,Fs = wollastonite, enstatite, and ferrosilite end-members in pyroxene; Al,Py,Sp,Gr = almandine, pyrope, spessartine, and grossular contents of garnet; Ms = Si atoms per formula unit of muscovite; Ep = pistacite content of epidote; Chl = Mg# of chlorite; Zeol = zeolite.

Table 2
Representative compositions of amphiboles

Sample	C142	C142	C153	O21	O25	O25	O33	O32	O30	O30	O31
Name	ac	pghb	pghb	sthb	edhb	ac	edhb	ed	ac	pghb	hhsthb
SiO_2	54.05	41.43	42.12	43.12	47.30	54.40	44.54	47.42	53.55	44.32	45.40
Al_2O_3	3.79	12.96	12.82	11.42	10.65	4.00	11.97	9.82	4.57	13.25	12.17
TiO_2	0.12	1.53	2.19	0.93	0.45	0.12	0.49	0.27	0.10	0.46	0.26
FeO*	9.49	16.56	15.22	17.52	11.35	7.58	17.03	13.58	11.79	14.29	14.92
Cr_2O_3	0.07	0.10	0.10	0.12	0.37	<	0.04	<	0.27	0.07	<
MnO	0.28	0.75	0.14	0.30	0.24	0.23	0.32	0.37	0.20	0.26	0.28
MgO	17.14	9.02	10.39	10.05	14.31	19.12	10.27	13.48	15.78	11.17	11.46
CaO	12.69	11.94	11.51	11.84	11.86	12.20	10.96	10.87	12.11	11.56	11.07
Na_2O	0.38	1.78	1.69	1.56	1.47	0.61	2.00	2.00	0.51	1.77	1.87
K_2O	0.11	1.26	1.46	0.90	0.42	<	0.36	0.23	0.12	0.40	0.29
Sum	98.11	97.33	97.64	97.76	98.42	98.29	97.98	98.04	99.00	97.55	97.73
Si	7.61	6.27	6.27	6.42	6.72	7.52	6.52	6.78	7.54	6.46	6.58
Al^{IV}	0.39	1.73	1.73	1.58	1.28	0.48	1.48	1.22	0.46	1.54	1.42
Al^{VI}	0.24	0.59	0.52	0.43	0.50	0.17	0.58	0.43	0.29	0.74	0.65
Ti	0.01	0.17	0.25	0.10	0.05	0.01	0.05	0.03	0.01	0.05	0.03
Fe^{3+}	0.18	0.14	0.26	0.52	0.55	0.44	0.72	0.81	0.25	0.50	0.70
Cr	0.01	0.01	0.01	0.01	0.04	<	0.00	<	0.01	0.01	<
Fe^{2+}	0.94	1.96	1.63	1.67	0.80	0.44	1.36	0.81	1.13	1.24	1.11
Mn	0.03	0.10	0.02	0.04	0.03	0.03	0.04	0.04	0.02	0.03	0.03
Mg	3.59	2.04	2.31	2.23	3.03	3.94	2.24	2.87	3.31	2.43	2.47
Ca	1.91	1.94	1.84	1.89	1.81	1.81	1.72	1.66	1.83	1.81	1.72
Na^{M4}	0.09	0.06	0.16	0.11	0.19	0.16	0.28	0.34	0.14	0.19	0.28
Na^{A}	0.02	0.46	0.33	0.34	0.21	<	0.28	0.22	0.00	0.31	0.24
K	0.02	0.24	0.28	0.17	0.08	0.01	0.07	0.04	0.02	0.07	0.05

Where substantially different, core and rim compositions are shown separately. < = below detection. Cations calculated assuming total cations: $(Ca + Na + K) = 13$, $Na^{M4} = 7 - (Ca + Fe + Mg + Mn + Al^{VI} + Ti + Cr)$, and $Na^{A} = Na - Na^{M4}$. ac = actinolite; pghb = (ferroan/ferro-) pargasitic hornblende; hsthb = (magnesio/magnesian-) hastingsitic hornblende; hst = (magnesio/magnesian-) hastingsite; edhb = edenitic hornblende; ed = edenite. Analyses made at Stanford and UCLA, using an accelerating voltage of 15 kV, 15 nA sample current, and 2 μm beam size.

tion by diffusion at elevated temperature. Most garnet rims show increased Fe and/or Mn and decreased Mg (Fig. 6), suggesting late modification of the garnet by an exchange or net-transfer reaction. This zoning is most pronounced at grain margins in contact with adjacent or included clinopyroxene crystals, and is likely the result of Fe and Mg exchange between garnet and clinopyroxene [17].

Garnet occurs throughout the metasedimentary rocks at Tayin. Most are 30–60 μm in diameter, although a few samples contain garnets as coarse as 250 μm. There is no relation between garnet grain size and structural position within the sole. The metasedimentary garnets are MnO-rich, with a typical composition $Alm_{50}Pyr_{13}Grs_{09}Sps_{27}$. They are strongly zoned, reflecting decreasing Mn and increasing Fe uptake during growth (Fig. 6). The zoning indicates growth at conditions insufficient for homogenization by diffusion, either at temperatures below 600°C [18] or during short periods of heating. Metasedimentary and mafic garnet compositions are similar to those reported by Searle and Malpas [11] and Ghent and Stout [3].

5.5. Mica

Muscovite occurs in metasedimentary rocks as a peak metamorphic phase, and in mafic rocks as a retrograde alteration of plagioclase. Si atoms per formula unit range from 3.1 to 3.4 for metasedimentary and from 3.1 to 3.3 for mafic rocks. None of the micas examined were compositionally zoned. Biotite was found in only two samples, as an alteration product of hornblende.

Table 3
Compositions of garnet and clinopyroxene crystals and calculated temperatures and pressures

	Garnet				Clinopyroxene				Temperature (°C)			
	Ca	Fe	Mg	Mn	Ca	Fe	Mg	K_D	G&A	R&G	E&G	P&N
O56												
core	0.70	1.52	0.68	0.10	0.85	0.35	0.64	4.09	704	751	877	814
rim	0.66	1.56	0.62	0.15	0.9	0.36	0.66	4.61	677	719	825	751
incl.	0.70	1.52	0.68	0.10	0.86	0.37	0.62	3.75	752	776	908	867
incl.	0.64	1.64	0.59	0.13	0.86	0.34	0.69	5.64	614	670	758	656
incl.	0.69	1.52	0.69	0.12	0.86	0.37	0.62	3.69	758	780	909	868
incl.	0.71	1.53	0.63	0.10	0.87	0.35	0.67	4.65	676	717	839	764
rim	0.62	1.65	0.57	0.13	0.86	0.35	0.66	5.46	623	677	764	668
C139												
rim	0.54	1.70	0.68	0.06	0.82	0.33	0.73	5.53	617	674	736	616
rim	0.52	1.69	0.75	0.05	0.84	0.32	0.71	5.00	646	699	758	637
rim	0.52	1.68	0.75	0.05	0.82	0.32	0.74	5.18	636	690	748	621
rim	0.55	1.65	0.75	0.04	0.83	0.32	0.74	5.09	642	694	762	639
rim	0.52	1.67	0.77	0.04	0.82	0.32	0.72	4.88	654	705	765	643
incl.	0.51	1.70	0.74	0.04	0.84	0.34	0.69	4.66	668	716	777	672
core	0.53	1.68	0.74	0.04	0.83	0.37	0.66	4.05	717	754	828	754
rim	0.52	1.73	0.69	0.02	0.86	0.37	0.67	4.54	677	723	789	704
rim	0.52	1.71	0.72	0.01	0.84	0.36	0.67	4.42	686	730	798	711
core	0.53	1.71	0.71	0.05	0.86	0.36	0.7	4.68	667	715	781	684
C153												
core	0.70	1.57	0.65	0.07	0.89	0.32	0.66	4.98	653	700	813	723
rim	0.68	1.58	0.65	0.08	0.89	0.33	0.69	5.08	646	695	801	706
core	0.73	1.53	0.66	0.09	0.87	0.33	0.64	4.50	687	726	853	779
rim	0.74	1.55	0.62	0.08	0.86	0.35	0.67	4.79	667	710	838	764
core	0.92	1.46	0.53	0.09	0.88	0.31	0.66	5.86	611	661	826	750
rim	0.80	1.53	0.59	0.08	0.88	0.3	0.66	5.71	615	667	800	708
core	0.58	1.54	0.78	0.10	0.88	0.34	0.7	4.06	717	753	842	744
rim	0.53	1.66	0.60	0.14	0.89	0.34	0.7	5.70	608	668	728	613
core	0.59	1.52	0.79	0.10	0.89	0.31	0.71	4.41	690	731	818	698
rim	0.78	1.47	0.66	0.08	0.87	0.31	0.7	5.03	653	697	834	738
rim	0.66	1.53	0.74	0.07	0.86	0.32	0.68	4.39	693	732	840	743
rim	0.70	1.55	0.66	0.08	0.86	0.31	0.68	5.15	643	691	803	703
rim	0.74	1.52	0.66	0.07	0.88	0.3	0.69	5.30	635	685	806	703
rim	0.68	1.52	0.72	0.07	0.89	0.3	0.7	4.93	656	702	811	699
O156												
	0.94	1.44	0.47	0.15	0.88	0.32	0.65	6.34	589	643	809	732
	0.97	1.43	0.46	0.14	0.84	0.34	0.64	5.90	611	660	839	776
	0.67	1.52	0.74	0.07	0.87	0.30	0.67	4.61	677	719	827	719
	0.70	1.51	0.72	0.07	0.90	0.31	0.68	4.59	680	720	839	742

Pressures calculated at 700°C for comparison purposes. G&A = Green and Adam [26]; R&G = Raheim and Green [25]; E&G = Ellis and Green [23]; P&N = Pattison and Newton [24]. Core = core compositions of adjacent phases; rim = rim compositions of adjacent phases; incl = compositions of pyroxene included in garnet.

5.6. Ca–Al hydrosilicates

Ca–Al hydrosilicates present in the sole include xonotlite [3], epidote, pumpellyite ($Ca_{3.8}Mg_{0.9}Fe^{2+}_{0.1}Fe^{3+}_{0.5}Al_{4.4}Si_{6.1}O_{22}(OH)_7$)–$Ca_{3.8}Mg_{0.3}Fe^{2+}_{0.7}Al_{5.0}Si_{6.1}O_{22}(OH)_7$), prehnite, and zeolites. Epidote crystals have variable compositions ranging from 2 mol% to 29 mol% pistacite. Some exhibit clearly prograde (coarse crystals intergrown with hornblende and plagioclase) or retrograde (fine

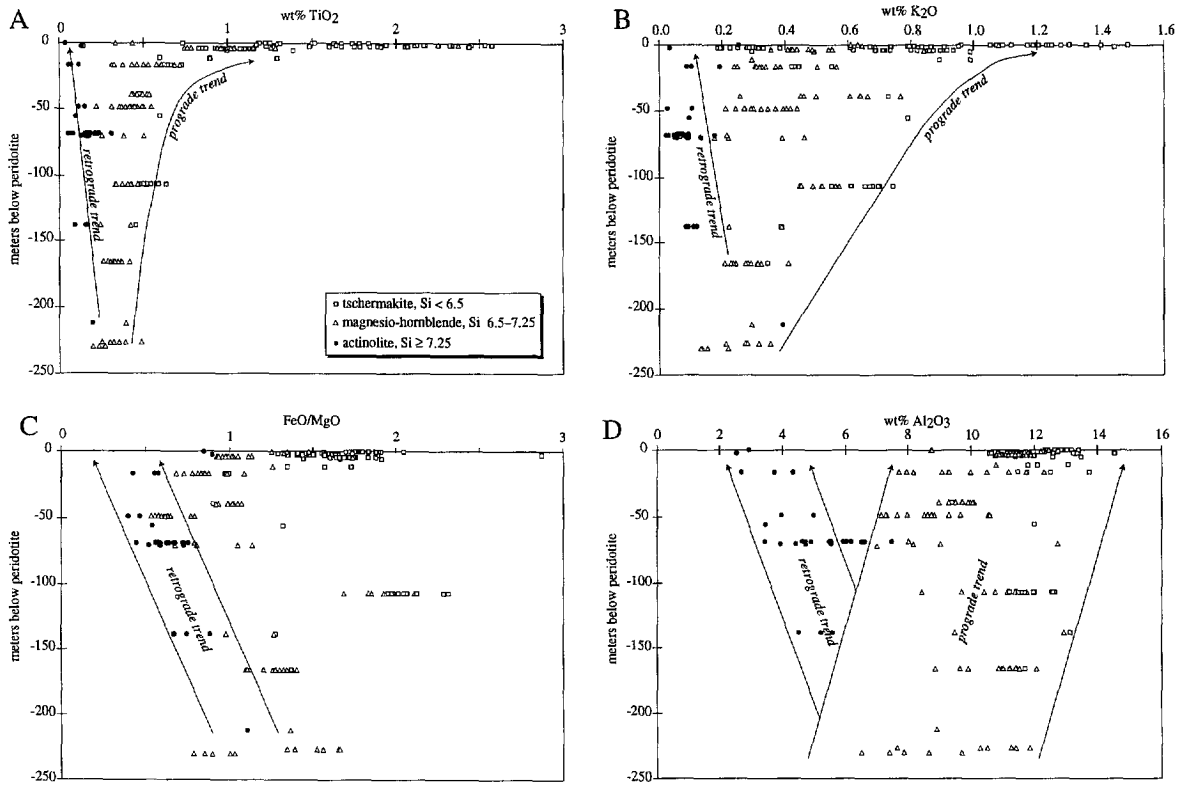

Fig. 5. Changes in hornblende composition within the metamorphic sole at Wadi Tayin. Symbols indicate variations in Si content, which allow differentiation of prograde (unfilled) and retrograde (filled) amphiboles. Inferred prograde compositional trends (increasing TiO_2, K_2O, and Al_2O_3) and retrograde compositional trends (decreasing TiO_2, K_2O, FeO/MgO and Al_2O_3) are shown with arrows.

crystals replacing plagioclase) textures, whereas others are ambiguous. This is the first report of pumpellyite from the sole of the Samail ophiolite.

Alteration of peak metamorphic phases to Ca–Al hydrosilicates is strongest in the upper part of the section. Within 20 m of the peridotite, alteration of

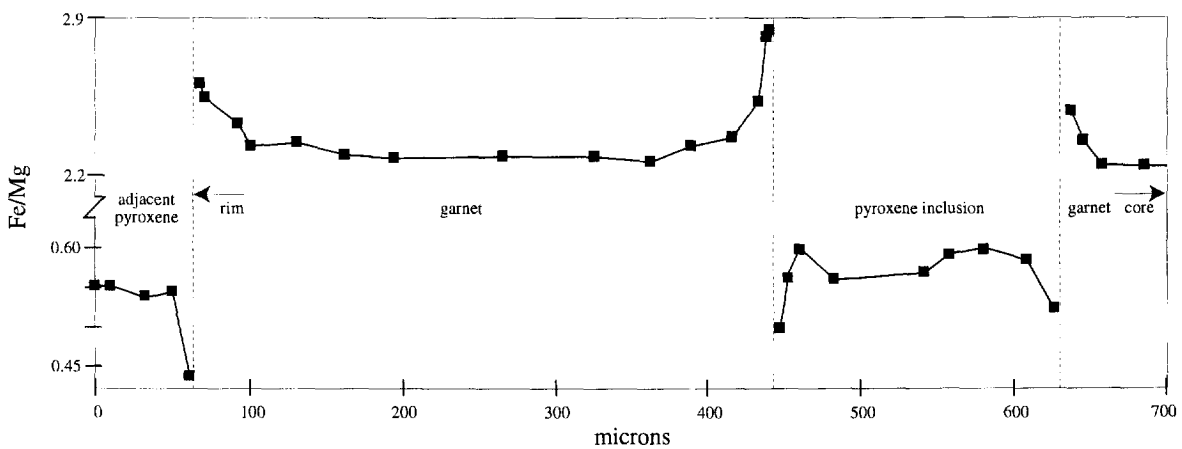

Fig. 6. Fe/Mg profile through garnet and clinopyroxene zoning in sample O56 demonstrates, for both phases, homogeneity of grain cores and zoning along grain boundaries.

plagioclase to albite + epidote + muscovite is noticeably more advanced, and within 3–4 m of the contact plagioclase is completely replaced by albite + prehnite + pumpellyite. In this same zone, hornblende is pervasively replaced by chlorite in some samples. Retrograde epidote is widespread as an alteration product of plagioclase, and epidote-filled veins are more abundant in the upper part of the section nearest the peridotite.

5.7. Fe and Ti oxides and sulfides

It is often difficult to assess whether oxide phases are in equilibrium because of their typical euhedral, porphyroblastic habit. The prograde minerals observed are ilmenite, magnetite, and rutile (Table 1); hematite is exclusively a retrograde phase. Pyrite was found in two garnet- and clinopyroxene-bearing samples from the uppermost portion of the sole.

6. Discussion

6.1. Conditions of metamorphism

Conditions of metamorphism were estimated using observed mineral parageneses (Table 1) and compositions (Tables 2 and 3). Aside from a single garnet–clinopyroxene temperature estimate from Sumeini, all the inferences below were derived from observations made at Tayin.

All mafic rocks in the sole contained prograde hornblende and intermediate composition plagioclase. Thus, minimum prograde temperatures are at least 475°C and perhaps as high as 550°C [19]. Prograde epidote, which is present at the 5–20% level in most rocks, is first absent 43 m below the peridotite, and disappears entirely within 15–20 m of the top of the section (Fig. 3B). Experiments [20] suggest that the disappearance of epidote + quartz at 400–600 MPa takes place at 590–660°C, depending on pressure and oxygen fugacity. Prograde chlorite is present in excess of 10 vol% in the lower 10 m of the section, diminishes to less than 5 vol% within 150 m of the peridotite, is first absent 74 m below the peridotite, and disappears entirely within 24–31 m of the top of the section; chlorite disappears in experimentally heated basalt at 550–575°C [21]. The presence of clinopyroxene indicates that temperatures within the upper 2 m of the sole were ≥ 780°C if the oxygen fugacity was equivalent to the quartz–fayalite–magnetite buffer [22], as suggested by the presence of ilmenite.

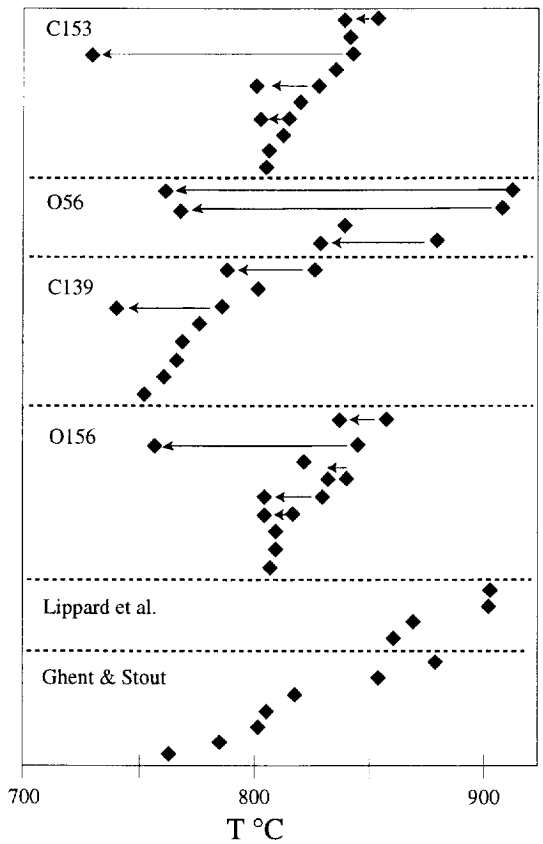

Fig. 7. Calculated garnet–clinopyroxene temperatures based on Fe/Mg partitioning [23,27] suggest temperatures in the range of 775–875°C. Arrows show effects of core to rim compositional differences. 'Lippard et al.' and 'Ghent and Stout' indicate temperatures calculated using compositions published by [2] and [3], respectively. Vertical positioning of data is for clarity and has no physical significance.

Previous investigators have used the partitioning of Fe and Mg between garnet and clinopyroxene to calculate metamorphic temperatures. A number of calibrations are available, based on four different experimental data sets [23–26] (Fig. 7). Berman et al. [27] re-evaluated the thermodynamic properties of garnet and clinopyroxene end-members and the mixing properties of these phases using Pattison and Newton's experimental data with expanded uncertainties; their calibration is essentially identical to

Ellis and Green's. We measured Fe/Mg partitioning between clinopyroxene and almandine-rich garnets. Zoning profiles were obtained for several garnets from each of four rocks. Each chosen garnet was adjacent to and/or included clinopyroxene grains. Zoning profiles were also obtained for one or more of these clinopyroxene crystals. Where possible, zoning profiles were also obtained for garnet isolated from other ferromagnesian phases. With these data we were able to characterize compositional zonation and evaluate whether the zonation developed during growth or during retrograde exchange with adjacent phases. Zoning was not detected in clinopyroxene crystals except rarely near adjacent garnet crystals, where Ca showed a slight increase (Fig. 6). Virtually all garnets adjacent to clinopyroxene grains show decreasing Mg, increasing Mn, and increasing Fe toward the margin (Fig. 6). Fig. 7 illustrates that, for an assumed pressure of 500 MPa, temperatures range from 775° to 875°C, centering on ~ 825°C, similar to earlier reports [3,11].

Garnet–hornblende pairs [28] from Oman yield temperatures of 650–875°C, with the bulk of the estimates between 675° and 775°C (Fig. 8). Three samples contain garnet + clinopyroxene + hornblende. In two of these samples, O56 and C139, the garnet–hornblende temperatures are ~ 100°C lower than the garnet–pyroxene temperatures, whereas the temperatures for C153 are ~ 50°C higher.

Estimating physical conditions of the greenschist and prehnite–pumpellyite facies overprint(s) is difficult because of the generally poor understanding of phase relations and the disequilibrium common at low temperatures. Greenschist facies minerals increase markedly in abundance up-section and reach their apex just beneath the peridotite. This suggests

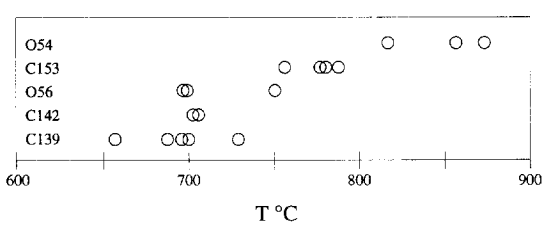

Fig. 8. Garnet–hornblende temperatures calculated using Graham and Powell [28] range from ~ 700–850°C. Vertical positioning of data is for clarity and has no physical significance.

that their crystallization was driven by the influx of fluid from the serpentinized peridotite above or from fluids channelled along the peridotite/sole fault. The most common greenschist facies assemblage in the mafic sole rocks is albite + actinolite + K-feldspar + epidote + K-white mica + chlorite + sphene + calcite ± hematite ± pumpellyite ± calcite. The coexistence of actinolite + epidote + pumpellyite is compatible with metamorphic pressures of 200–400 MPa and temperatures of 150–350°C [29]. Within a few meters of the peridotite, albite, actinolite, epidote, pumpellyite, prehnite, K-white mica, chlorite, sphene, calcite, and zeolites are found in the same rock. The restriction of prehnite and zeolites to these upper few meters suggests that these minerals overprint the greenschist facies assemblage. Regardless, the presence of zeolites and prehnite suggest temperatures < 200°C and maximum pressures of a few hundred MPa [30].

6.2. Shape of the temperature and displacement gradient

One of the most remarkable aspects of ophiolites emplaced onto continental margins is that their metamorphic soles have been reported to contain inverted metamorphic gradients of > 1000°C/km over a few hundreds of meters. Such steep inverted metamorphic gradients pose a problem because they are a factor of 10 greater than inverted thermal gradients produced by conventional thermal models of subduction zones or other thrust faults [31]. As discussed by Hacker [12,13], the shape of the gradient carries significant information about the deformation of the sole during ophiolite emplacement and about the age of the ophiolite at the time of emplacement. The data presented here constrain the shape of the inverted metamorphic gradient.

If the inverted metamorphic gradient were linear, the sole would show peak metamorphic temperatures that increase linearly up-section. However, at Tayin the changes in hornblende composition (e.g., Ti), mineral assemblages (decrease and loss of epidote and chlorite), preservation of Mn zoning in metasedimentary garnet, and calculated peak metamorphic temperatures, suggest an exponential gradient (Fig. 9a). Although the peak temperature gradient aver-

ages about 1000°C/km, it varies from ~ 100°C/km in the bottom half of the sole to ≥ 4000°C/km in the upper 50 m (Fig. 9A). Conventional thermal models of subduction zones and other thrust faults (e.g., [31]) produce inverted temperature gradients of 100°C/km or less. Thus, the lower 150 m of the sole

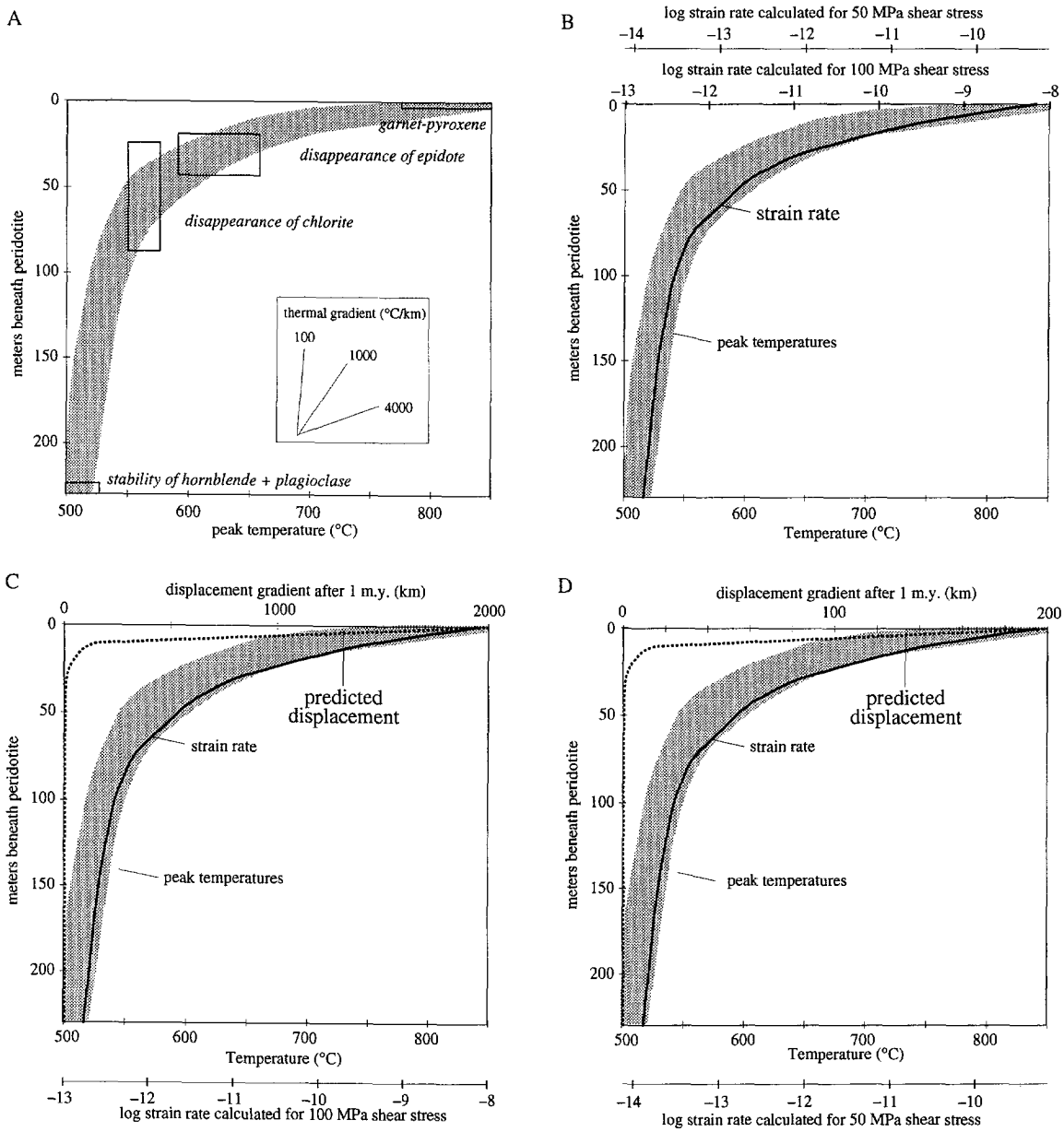

Fig. 9. (A) Observed mineral assemblages and calculated temperatures are combined to infer a non-linear gradient in peak metamorphic temperatures. (B) Strain rates calculated using an amphibolite flow 'law' are 10^{-12}–10^{-14} s^{-1} for most of the profile, only reaching 10^{-9} s^{-1} in the upper few meters. (C) and (D) Displacement profiles calculated by integrating the strain rate gradients, assuming (C) 100 MPa differential stress or (D) 50 MPa differential stress. The predicted displacement is essentially zero in the lower 225 m and 95% of the predicted displacement is in the upper 25 m.

in Oman plausibly represent a discrete block of only weakly deformed material and the inverted metamorphic gradient within those 150 m may be equivalent to an inverted thermal gradient present during thrusting. In contrast, the upper 50–100 m of the sole must have formed by a different mechanism.

The sole of the Oman ophiolite is a composite formed of rocks that, with increasing structural depth beneath the peridotite, came from progressively greater distances from their present position [13]. The rocks immediately beneath the peridotite travelled the shortest distance and the lowest rocks in the sole travelled the farthest relative to the peridotite. With some simplifying assumptions it is possible to calculate this displacement gradient using a flow 'law' for amphibolite. Thermomechanical modelling suggests that the shear stress during ophiolite emplacement was ~ 100 MPa [13]. This stress can be used to calculate a strain rate profile through the sole (Fig. 9B) using an amphibolite constitutive relationship [32] and converting from uniaxial shortening to simple shear [33]. As expected, the strain-rate gradient tracks the temperature gradient as $exp(1/T)$. The magnitude of the strain rate is subject to a great deal of uncertainty, conservatively ± 3 log units, deriving from the fit of the experimental data to the constitutive relationship and the extrapolation of the experimental results to natural strain rates that are 2–6 orders of magnitude slower. Fig. 9B also shows the strain rate profile that results if a shear stress of 50 MPa is assumed. In this case the strain rates are essentially an order of magnitude slower.

With these caveats in mind, the vertical strain-rate gradient through the sole can be integrated in space and time to provide a displacement profile. The displacement, u, is given by:

$$u = \int_0^z \int_0^t \dot{\gamma} \, dt \, dz$$

where z is depth, t is time, and $\dot{\gamma}$ is strain rate. Hacker et al. [34] demonstrated with $^{40}Ar/^{39}Ar$ dating that deformation of the sole lasted ~ 1 m.y. The displacement profiles calculated by integrating the strain-rate gradient of Fig. 9B over 1 m.y. are shown in Fig. 9C (for 100 MPa stress) and Fig. 9D (50 MPa stress). Although the absolute displacements are not well constrained, Fig. 9D agrees with palinspastic reconstructions of thrust sheet geometries [9], which suggest that the ophiolite thrust sheet (including the sole) was displaced ~ 150 km over the underlying Umar Group. The salient aspect of the predicted displacement gradient is that 99% of the total displacement occurred within the upper 25 m, and the lower 200 m of the sole arrived as nearly an intact block with less than 2 km of relative displacement from top to bottom. In Fig. 9C this implies shear strains of ~ 8,000 in the upper 25 m of the sole and only ~ 10 in the lower 200 m.

This way of thinking about the formation of the inverted metamorphic gradient and the shear within the sole has important limitations. First, the calculations assume that the entire sole is amphibolite, whereas in reality other, weaker lithologies are present that would have taken up some of the strain and produced jumps in the displacement gradient. Second, the displacement gradient within the sole is assumed to result from smoothly varying simple shear, whereas inhomogeneities in the flow field, including zones of concentrated deformation and non-plane strain, assuredly occurred in nature.

7. Conclusions

At its classic exposure, Wadi Tayin, the metamorphic sole beneath the Samail ophiolite consists of ~ 230 m of lower to upper amphibolite facies mafic and quartzose tectonite. Greenschist facies rocks are absent, although the entire sole, particularly the upper half, was overprinted by greenschist-facies retrogression. The sole itself is structurally coherent, although its upper and lower contacts are faults. Changes in hornblende composition, the disappearance of chlorite and epidote, and calculated garnet–clinopyroxene and garnet–hornblende temperatures document that the inverted peak temperature gradient is ~ 100°C/km in the lower 150 m of the sole and steepens exponentially to > 4000°C/km in the upper 50 m. With an amphibolite constitutive relation and an assumed stress, a strain-rate gradient and displacement gradient were calculated. These calculated gradients reveal that the lower 200 m of the sole may be a discrete, relatively undeformed block from the subduction zone beneath the ophiolite, whereas the upper 25 m represent material originally

separated by tens to a couple of hundred kilometers now integrated into a single column.

Acknowledgements

Hilal Bin Mohammed Al-Azri, Director of the Geological Survey, Ministry of Petroleum and Minerals, Sultanate of Oman, provided lightning fast expert logistical support. Robert Coleman and Aley El-Shazly kindly helped get the project rolling. Mike Searle was very generous with maps and directions. Tjerk Peters provided helpful reprints. Hacker was funded by NSF grant EAR-9204741, and Mosenfelder was supported by the McGee and Shell funds at Stanford University and by a GSA Penrose Grant. Reviewed by W.G. Ernst, E. Gnos, J. Hawkins, C. Hopson, and J.G. Liou. *[MK]*

References

[1] F. Boudier, J.L. Bouchez, A. Nicolas, M. Cannat, G. Ceuleneer, M. Miseri and R. Montigny, Kinematics of oceanic thrusting in the Oman ophiolites: model of plate convergence, Earth Planet. Sci. Lett. 75, 215–222, 1985.

[2] S.J. Lippard, A.W. Shelton and I.G. Gass, The Ophiolites of Northern Oman, 178 pp., Geol. Soc. London, 1986.

[3] E.D. Ghent and M.Z. Stout, Metamorphism at the base of the Samail ophiolite, southeastern Oman Mountains, J. Geophys. Res. 86, 2557–2571, 1981.

[4] J.A. Pearce, T. Alabaster, A.W. Shelton and M.P. Searle, The Oman ophiolite as a Cretaceous arc-basin complex: evidence and implications, Philos. Trans. R. Soc. London A 300, 299–317, 1981.

[5] M. Ernewein, C. Pflumio and H. Whitechurch, The death of an accretion zone as evidenced by the magmatic history of the Sumail ophiolite (Oman), Tectonophysics 151, 247–274, 1988.

[6] C. Pflumio, Evidences for polyphased oceanic alteration of the extrusive sequence of the Semail ophiolite from the Salahi block (northern Oman), in: Ophiolite Genesis and Evolution of the Oceanic Lithosphere, T. Peters, A. Nicolas and R.G. Coleman, eds., Petrology and Structural Geology 5, pp. 313–352, Kluwer, Dordrecht, 1991.

[7] M.P. Searle and J. Malpas, Structure and metamorphism of rocks beneath the Semail ophiolite of Oman and their significance in ophiolite obduction, Trans. R. Soc. Edinburgh 71, 247–262, 1980.

[8] F. Boudier, G. Ceuleneer and A. Nicolas, Shear zones, thrusts and related magmatism in the Oman ophiolite: Initiation of thrusting on an oceanic ridge, Tectonophysics 151, 275–296, 1988.

[9] F. Bechennec, J. Le Metour, D. Rabu, C. Bourdillon-de-Grissac, P. de Wever, M. Beurrier and M. Villey, The Hawasina Nappes; stratigraphy, palaeogeography and structural evolution of a fragment of the South-Tethyan passive continental margin, in: The Geology and Tectonics of the Oman Region, A.H.F. Robertson, M.P. Searle and A.C. Ries, eds., Geol. Soc. London Spec. Publ. 49, 213–223, 1990.

[10] A.H.F. Robertson, M.P. Searle and A.C. Ries, eds., The Geology and Tectonics of the Oman Region, Geol. Soc. London Spec. Publ. 49, 845 pp., 1990.

[11] M.P. Searle and J. Malpas, Petrochemistry and origin of sub-ophiolitic metamorphic and related rocks in the Oman Mountains, J. Geol. Soc. London 139, 235–248, 1982.

[12] B.R. Hacker, Simulation of the metamorphic and deformational history of the metamorphic sole of the Oman ophiolite, J. Geophys. Res. 95, 4895–4907, 1990.

[13] B.R. Hacker, The role of deformation in the formation of metamorphic field gradients: Ridge subduction beneath the Oman ophiolite, Tectonics 10, 455–473, 1991.

[14] F. Allemann and T. Peters, The ophiolite–radiolarite belt of the North Oman Mountains, Eclog. Geol. Helv. 65, 657–697, 1972.

[15] F. Boudier and R.G. Coleman, Cross section through the peridotite in the Samail ophiolite, southeastern Oman Mountains, J. Geophys. Res. 86, 2573–2592, 1981.

[16] P. Raase, Al and Ti contents of hornblende, indicators of pressure and temperature of regional metamorphism, Contrib. Mineral. Petrol. 45, 231–236, 1974.

[17] R.J. Tracy, P. Robinson and A.B. Thompson, Garnet composition and zoning in the determination of temperature and pressure of metamorphism, central Massachusetts, Am. Mineral. 61, 762–775, 1976.

[18] S. Chakraborty and J. Ganguly, Compositional zoning and cation diffusion in aluminosilicate garnets, in: Diffusion, Atomic Ordering, and Mass Transport, Advances in Physical Geochemistry 8, J. Ganguly, ed., pp. 120–175, Springer, Berlin, 1990.

[19] F.S. Spear, Metamorphic Phase Equilibria and Pressure–Temperature–Time Paths, 799 pp., Mineral. Soc. Am., Washington, DC, 1993.

[20] J.G. Liou, Synthesis and Stability Relations of Epidote, $Ca_2Al_2FeSi_3O_{12}(OH)$, J. Petrol. 14, 381–413, 1973.

[21] M.J. Apted and J.G. Liou, Phase relations among greenschist, epidote amphibolite, and amphibolite in a basaltic system, Am. J. Sci. 283-A, 328–354, 1983.

[22] F.S. Spear, An experimental study of hornblende stability and compositional variability in amphibolite, Am. J. Sci. 281, 697–734, 1981.

[23] D.J. Ellis and D.H. Green, An experimental study of the effect of Ca upon garnet–clinopyroxene Fe–Mg exchange equilibria, Contrib. Mineral. Petrol. 71, 13–22, 1979.

[24] D.R.M. Pattison and R.C. Newton, Reversed experimental calibration of the garnet–clinopyroxene Kd (Fe–Mg) exchange thermometer, Contrib. Mineral. Petrol. 101, 87–103, 1988.

[25] A. Råheim and D.H. Green, Experimental determination of the temperature and pressure dependence of the Fe–Mg

partition coefficient for coexisting clinopyroxene and garnet, Contrib. Mineral. Petrol. 48, 179–203, 1974.

[26] T.H. Green and J. Adam, Assessment of the garnet–clinopyroxene Fe–Mg exchange thermometer using new experimental data, J. Metamorph. Geol. 9, 341–347, 1991.

[27] R.G. Berman, L.Y. Aranovich and D.R.M. Pattison, Reassessment of the garnet–clinopyroxne Fe–Mg exchange thermometer: II. Thermodynamic analysis, Contrib. Mineral. Petrol. 119, 30–42, 1995.

[28] C.M. Graham and R. Powell, A garnet–hornblende geothermometer; calibration, testing, and application to the Pelona Schist, Southern California, J. Metamorph. Geol. 2, 13–31, 1984.

[29] B.R. Hacker and J.W. Goodge, Comparison of Early Mesozoic high-pressure rocks in the Klamath Mountains and Sierra Nevada, in: Paleozoic and Early Mesozoic Paleogeographic Relations; Sierra Nevada, Klamath Mountains, and Related Terranes, D.S. Harwood and M.M. Miller, eds., Geol. Soc. Am. Spec. Pap. 255, 277–296, 1990.

[30] J.G. Liou, S. Maruyama and M. Cho, Very low-grade metamorphism of volcanic and volcaniclastic rocks — mineral assemblages and mineral facies, in: Low Temperature Metamorphism, M. Frey, ed., pp. 59–112, Blackie, Glasgow, 1987.

[31] S.M. Peacock, Creation and preservation of subduction-related inverted metamorphic gradients, J. Geophys. Res. 92, 12763–12781, 1987.

[32] B.R. Hacker and J.M. Christie, Brittle/ductile and plastic/cataclastic transitions in experimentally deformed and metamorphosed amphibolite, Am. Geophys. Union Monogr. 56, 127–147, 1990.

[33] S.M. Schmid, R. Panozzo and S. Bauer, Simple shear experiments on calcite rocks; rheology and microfabric, J. Struct. Geol. 9, 747–778, 1987.

[34] B.R. Hacker, J.L. Mosenfelder and E. Gnos, Rapid ophiolite emplacement constrained by geochronology and thermal considerations, Tectonics, in press.

[35] N.I. Christensen and J.D. Smewing, Geology and seismic structure of the northern section of the Oman ophiolite, J. Geophys. Res. 86, 2545–2555, 1981.

[36] M.H. Manghnani and R.G. Coleman, Gravity profiles across the Samail ophiolite, J. Geophys. Res. 86, 2509–2525, 1981.

[37] J.S. Pallister and C.A. Hopson, Samail ophiolite plutonic suite: field relations, phase variation, cryptic variation and layering, and a model of a spreading ridge magma chamber, J. Geophys. Res. 86, 2673–2645, 1981.